3D CRATER DATABASE PRODUCTION ON MARS BY AUTOMATED CRATER DETECTION AND DATA FUSION

J. I. Simpson [a,b] *, J.R Kim [b], J-P. Muller [b]

[a] QINETIQ Sundridge, Darenth House, 84 Main Road, Nr. Sevenoaks, Kent, TN14 6ER, UK
[b] Mullard Space Science Laboratory - Holmbury St. Mary - Dorking - Surrey - RH5 6NT, UK
jsimpson@qinetiq.com, jkim@mssl.ucl.ac.uk, jpm@mssl.ucl.ac.uk

WG VI/7

ABSTRACT:

Impact crater databases are a key resource for planetary geologists. Uses include studies of relative and absolute surface (age) chronologies, erosional processes, hydrological evolution and climate history. This paper describes the creation of 2D and 3D Mars crater databases from high resolution HRSC stereo imagery using data fusion and automated crater detection methods. A semi-automated process has been developed which incorporates a software GIS tool to facilitate the statistical assessment of detection rates and quality as well as provide 100% coverage with minimal human interaction. A specialized stereo matching system for impact craters using high quality HRSC stereo imagery with derived 2D crater boundaries was subsequently developed and applied. Using this tool, the best possible 3D profiles for various scale ranges were then extracted and cross verified using the 2D crater data. The algorithms which are demonstrated in this paper will provide a very powerful tool for future planetary studies.

1. INTRODUCTION

After more than four decades of research and manual efforts, only a few tens of thousands of the millions of craters on Mars have been catalogued, mainly those with diameters $\geq$ 5 km. Automated techniques for crater detection and cataloguing are therefore necessary to take advantage of the vast quantities of remotely sensed data now available, especially now that 3D information is routinely available from the ESA Mars Express HRSC instrument (Albertz et al., Scholten et al., 2005).

For the results of automated crater detection systems to be useful, high levels of accuracy must be achieved. This raises two immediate problems. Firstly, the accuracy of existing automated approaches is generally unsatisfactory and needs to be improved. Secondly, the lack of ground truth data makes it difficult to perform a meaningful and reasonably objective assessment. A further challenge is the development of a fully automated crater detection system capable of achieving accuracies $\geq 95\%$.

A number of databases of craters on Mars are readily available through the United States Geological Survey (USGS) website for the Planetary Interactive GIS Web Analyzable Database (PIGWAD) such as the Barlow catalogue containing 42,283 craters of diameters $\geq$ 5km. This was produced in the late 1980s from Viking 1:2,000,000 scale imagery with ≈231m/pixel resolution and is currently undergoing revisions to include Mars Global Surveyor and Mars Odyssey data (Barlow et al., 2003). Also available through PIGWAD are the Roddy catalogue of 4,300 craters $\geq$ 10km diameter, with morphological details; the Kuzmin catalogue and the Costard catalogue of 2,600 craters with fluidized ejecta blankets. All have crater diameters ≥5km.

The most important application field for reliable crater cataloguing and counting (using the Size Frequency Distributions) is the surface dating of planets. For example, surfaces on Mars have been subjected to a greater degree of modification than the Moon due to processes unique to Mars, such as water erosion. In addition to volcanic lava flows, there are areas of mobile sand dunes that obliterate smaller craters faster than larger ones, there is evidence of large-scale fluvial flows and ice movement with clear examples of surfaces that have been buried and/or exhumed. Whilst increasing the complexity, these dynamic processes can provide valuable information when analysed together with crater size-frequency distributions. Hartmann (1966) described how the age of a surface derived from crater counts is dependent both on the rate of crater formation and on the length of time that craters of that size last before evidence is lost due to erosion etc., Hartmann coined the term "crater retention age" as the average time interval that craters of a given size are retained on a surface.

There is general agreement that the Solar System experienced very high impact rates during a period from around 4.6 to 3.8 billion years ago, known as the "heavy bombardment", which then rapidly lessened and became relatively stable. This relatively stable cratering rate is the basis for surface dating techniques which use the distribution of sizes and counts of craters.

However, there are two problems to employ existing catalogues or in future more detailed catalogues for Martian chronology and geomorphological research. First of all, these catalogues focus on the larger craters, generally with diameters $\geq$ 5km, whilst the target diameter for the application of geological research is mainly from around a few hundred metres up to a few km, essentially covering the size frequency distribution below the Barlow catalogue.

The other problem is the deficiency of 3D information on craters. For research on erosional process over impact craters, the DTMs of corresponding crater is absolutely essential. The other need for 3D information is to enable the extraction of the depth-diameter ratio or the bottom shapes of crater. Secondary craters affect the dating of surfaces using crater counts since a single large primary impact can cause a great number of secondaries which will artificially increase the count and thus increase the age estimate.

---

* Corresponding author

One possible way to discriminate between secondary and primary craters is through depth-diameter information on each individual crater. Crater cataloguing with 3D data, has never been attempted before due to the lack of such high quality information but the authors consider this to be most worthwhile for such purposes as well as other research areas such as the physical mechanisms underlying impact crater formation. The release of HRSC stereo imagery makes this idea feasible. However, it is not easily achievable considering the relatively poor vertical accuracy of stereo DTMs, the limited resolution of raw stereo images and the contamination of HRSC image by compression errors. We address these problems by implementing a 3D stereo matching system incorporating re-constructed 2D crater boundaries derived from HRSC images.

2. ALGORITHMS

2.1 Algorithms for 2D crater data base extraction

There are a relatively small number of fundamental techniques underlying all of the automated crater detection systems which hav been developed to date. These can be classified into two broad groups, namely supervised and unsupervised. Supervised methods rely on machine learning from human input whereas unsupervised perform the detection process autonomously.

The unsupervised methods usually comprise three main algorithmic steps: 1) focusing, 2) feature extraction, 3) classification.

The focusing stage is aimed at reducing the computational cost required by differentiating between areas to be eliminated and areas to be processed further. Techniques for achieving this include edge detection, edge direction analysis and texture analysis. During feature extraction, all possible features are identified and selected from the results of the focusing stage. Most algorithms employ some form of Hough Transform to achieve this, although genetic algorithms are another possibility used by Cheng (2003),whilst Kim et al (2005) used conic section fitting. The final stage is to classify the output from the selection of candidate features. This involves a trade-off between over and under detection, the goal being to maximize detections while minimising false positives.

Supervised systems begin with a learning or training phase where examples of features being sought are fed to the algorithm. The algorithm is then applied to an unlabelled data set.

This research contains the following material re-organised and summarised from Kim et al (2005a) and Kim (2005) which both describe the algorithm in greater detail.

The 3 stages in the overall algorithm is as follows:
- a focusing stage to define target edge segments in regions of interest (ROIs)
- an organization stage to find optimal ellipses
- a refinement and verification stage to remove false detections

The focusing stage reduces the search space by extracting edge magnitude and direction using a Canny operator and then extracts regions of interest (ROIs) using a Grey Level Co-occurrence Matrix (GLCM) texture classification.

The organisation stage takes the preliminary crater rims created in the focusing stage and organises them into optimal ellipses using graph-based conic section fitting methods. First, the Direct Least Squares (DLS) fitting method (Fitzgibbon et al, 1996) is applied, as being the most computationally efficient. In the final fitting stage the osculating ellipse (OE) detection algorithm (Kanatani and Ohta, 2004) is used to find the best conic section from candidate craters.

Verification and refinement, the final stage, first refines the feature selections by employing a template matching scheme where the maximum correlation for each crater against pre-specified templates are chosen, provided they exceed a given threshold. The final operation is to remove false detections using eigencrater construction (Turk and Pentland, 1991) and neural network template recognition involving training vectors representing a set of craters and a set of non craters.

However, application of such a set of impact crater detection algorithms over a single image strip do not provide 2D crater GIS over extensive areas. For this, multiple image strips are required together with a merging process to compile the detection results together from individual images.

Adjacent images invariably have areas of overlap which means that most, if not all, craters detected in the overlap region will appear duplicated in the set of results for each image. These duplicates must be identified and resolved to a single crater. This could be done manually but the ultimate aim is total automation of the entire process, so a simple version of automated duplicate detection was needed. It is likely that the actual crater descriptions for duplicate craters will not be absolutely identical, due to variations between the images, algorithmic artefacts or co-registration issues. This means that two definitions of the same crater may differ in terms of the centre locations, the radii or both.

To incorporate craters from different catalogues, Salamuniccar and Loncaric (2007) proposed a simple function, very similar to that used in Vinogradova et al (2002), which relates diameter and radius such that variations in the most significant of either of these can be compared against a critical value and used to determine whether the definitions in each catalogue are likely to refer to the same crater. Their method consists of two stages: firstly, obtain a quantifiable measure of the differences between crater radii and centre point location and then compare this against some critical value. If the measure is less than some critical value then it is likely that a duplicate has been identified. This is formalised in the two equations below (Salamuniccar and Loncaric, 2007), both conditions of which must be satisfied.

$$f_m = \max\left(\frac{r_1}{r_2} - 1, \frac{d}{r_2} \right) \quad (1)$$
$$f_m < f_c$$

Where *fm* is the difference measurement factor, *r1* and *r2* are the radii, chosen such that *r1 > r2*; *d* is the distance between the crater centres and *fc* is the critical factor value.

The selection of a suitable critical factor is important. If the value is too high, too few duplicates or spurious duplicates will be found, and true duplicates will be missed. They suggest that the critical value should be less than the smallest value for the distance measurement factor *fm* found in either dataset. The distance or overlap between duplicates, although small, often exceeded that found internally within the data sets and so would result in duplicates not being correctly identified. A factor of 2.0 was found to be suitable. After a set of potential duplicates is identified, all possible combinations are tested and the two with the smallest distance/radius difference measure are resolved into a single crater using the mean centre and radius.

2.2 3D crater DTM extraction

For this purpose, we use the 2D crater boundary as *a priori* knowledge for stereo matching. The usual area-based stereo image matchers are not robust over the distorted surface. One possible solution is finding the estimated disparity surface using the approximate 3D shape of the impact crater. Then the image matching will be performed along the surface of the pre-

estimated 3D disparity shape. Therefore the procedure to extract 3D craters can be divided into two parts 1) estimation of an approximate 3D crater model, 2) image matcher implementation applied to the estimated disparities

2.2.1   Estimation of approximate 3D crater model

To reconstruct the modelled 3D shape of a crater, the fused data, which consist of a detected crater radius and centre as well as the DTM of the encircled area, are fitted to a height model. Duxbury (1991) suggested a 3D crater model as follows:

$$h(D,R) = -kD^2 \cos(\frac{R}{D}\pi) \qquad (2)$$

$$(0 < D < 2R)$$

otherwise

$$h(D,R) = 0$$

where R is the crater radius and D is the distance from the centre point.

However, the outer boundary of this model is not realistic for the purpose of stereo matching applications, therefore we employed a simple polynomial model in the normalized co-ordinate as shown below (it should be noted that all units in these models are dimensionless):

$$h(r_n) = \sum_{i=0}^{order} k_i r_n \qquad (3)$$

$$(0 < r_n < 2R),$$

where r_n is the normalised distance from the centre point ($r_n = D/R$) and k_n is the normalised model constants.

Then, the dimensionless shape of an impact crater can be simply transferred into its original shape by multiplying it with a normalisation factor which can then be extracted from the radial transect of stereo height. Figure 1 shows the process of normalised crater model fitting.

1pixel=20m
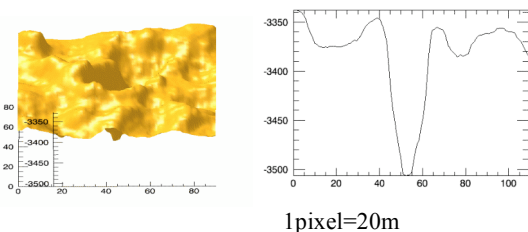
(a) Extracted crater DTM from HRSC stereo DTM (crater size =1km)

1pixel=20m
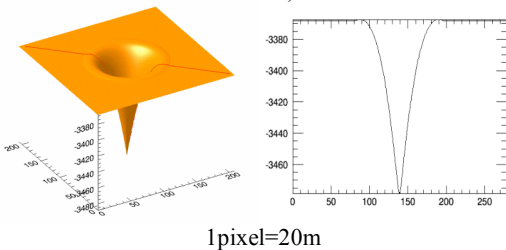
(c) Fitted crater model using 4th order polynomial and profile
Figure 1. Model fitting a stereo crater DTM using a polynomial model

Normally such crater models are extracted from wide area DTMs using 2D crater boundaries. However, it's not always possible to guarantee that HRSC stereo DTMs will have sufficiently low noise to calculate a 3D crater approximation with sufficient accuracy. Therefore, two kinds of 3D models, which represent flat bed centres and concave surfaces, were tested against 40 well constructed crater DTMs as follows:

$$h(r_n) = 0.11 + 1.23r_n - 0.70r_n^2 + 0.11r_n^3 + 0.01r_n^4 \qquad (4)$$

$$h(r_n) = 0.04 + 0.16r_n - 1.1r_n^2 + 3.99r_n^3 - 4.66r_n^4 + 1.75r_n^5$$

Initially, the fitted 3D models computed from the HRSC DTMs were compared with these two models using convolution. If the convolved values with either of these 3D models is below some threshold value, the crater is rejected as being unsuitable. In such a case, one of the models whose simulated hill shaded image has a higher correlation with the original optical image, is used to create the first base DTM model for the disparity estimation in the subsequent image matching process.

2.2.2   Stereo image matcher implementation

The starting point for the image matcher implementation is a spherically shaped y-disparity map in HRSC quasi-epi-polarity space as shown in Figure 2. The 3D polynomial crater model which was extracted from the stereo HRSC DTM or standard model and the boundary information of a 2D crater GIS was used to remove the expected image distortion for the ALSC (Adaptive Least Squares Correlation, Gruen, 1985) image matcher which is employed in this matching system for the higher sub-pixel accuracy. The weakness of the ALSC image matcher in concave shaped areas can be now successfully avoided.
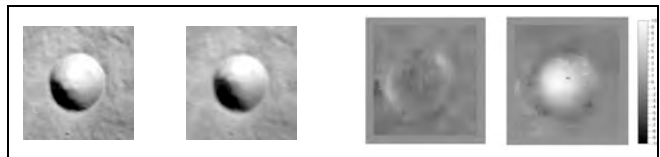
Figure 2. The stereo disparity of associated with the original DTM and the deviation from a model-fitted orthorectified image of an impact crater (R=500m)

The merits of this approach are obvious as shown in Figure 3. The crater DTM without a pre-defined 3D model shows a coarse shape where the rim and bottom part in the matching window are mixed up so some part of the height is overestimated or underestimated severely.
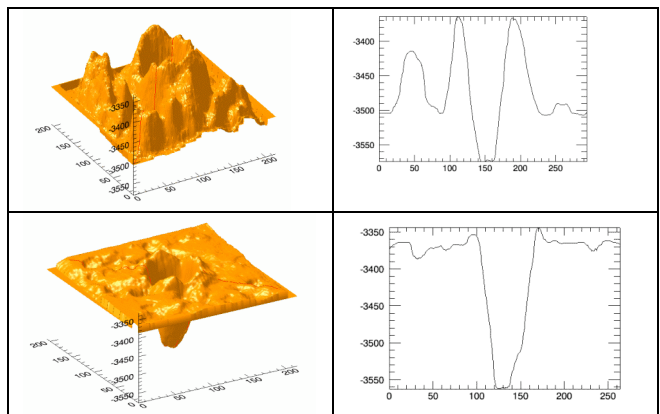
Figure 3. The 3D crater which is extracted from a zero base surface (z=0, upper) and the one from a pre-defined 3D crater model using the first case of eq (4), lower)

The other approach which is employed in the crater specific image matching system is to iterate using different matching window sizes. The iterative process starts with a maximum matching window size which can more easily avoid the local image artifacts and proceeds with a smaller patch which can be more reliable to reconstruct the detailed shape. At each iteration stage, the input images used by the image matchers are rectified using a 3D model by 3D intersection and polynomial fitting.

Figure 4 shows an evaluation of the crater DTMs at different iteration stages.

(a) First iteration (matching window 10)

(b) Second iteration (matching window 8)

(c) Third iteration (matching window size 6)

d) Final iteration (matching window size 4)
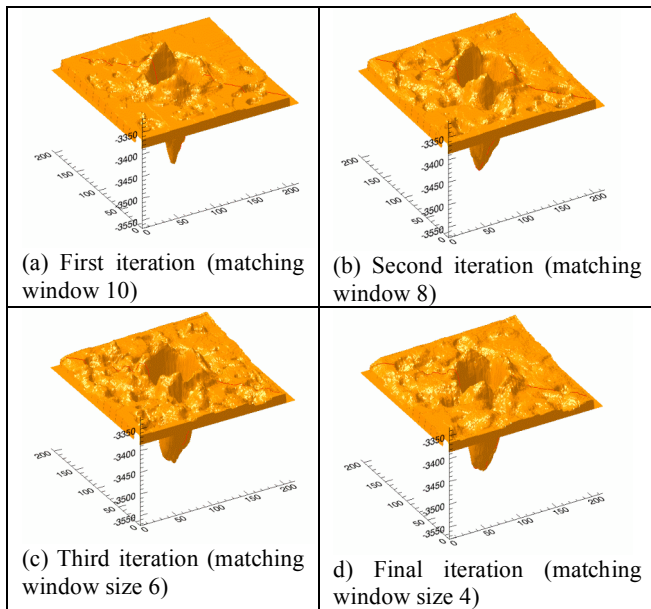
Figure 4. Crater DTM model fitting evolution at each iteration stage (1 pixel =20m)

3. RESULT AND ASSESSMENT

Two regions were selected for detailed study, Elysium Planitia (9-11ºN,148-158ºE) and Iani Vallis (0-7ºN, -14-19ºE). They were chosen for their geological interest and different topographies, Elysium being a flat frozen sea area (Murray et al., 2005) and Iani being a chaotic region with deep valleys and massive flood drainage (Gupta et al., 2008).
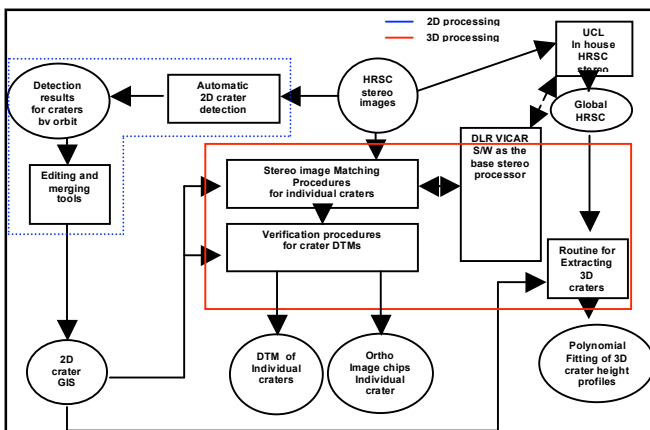
Figure 5. Overview of Crater processing system for 3D and 3D crater database generation

To process such large area data sets, the processing chain shown in Figure 5 was constructed. The photogrammetric processing such as 3D intersection and ortho image generation uses the DLR VICAR software which is available to HRSC team members and their associates (Scholten et al., 2005). At first, a wide area HRSC DTM up to 50m resolution and 40m ortho image sets was created and then a 2D crater GIS was processed by the processing chain, described in section 2.1. Then the 2D detection result and global DTM are fed forward into the 3D processing line which can automatically generate DTMs and ortho image "chips" of individual craters. The target range of crater processing is R≥ 400m for optical images. 3D processing was implemented in small areas such as HRSC image h2099

over Elysium and h9023 in Iani. However, the comprehensive 3D processing for both entire areas is still ongoing and will be shown in the final presentation.

3.1 Generation and assessment of 2D crater Database

A performance evaluation of the 2D craters was made using Building Detection Metrics (Shufelt, 1999). These were devised in order to provide an objective measure of performance for automated building detection algorithms, a situation analogous to automated crater detection:

$$Detection\ Percent = (100 * TP) / (TP + FN)$$
$$Branching\ Factor = FP / TP$$
$$Quality\ Percent = (100 * TP) / (TP + FN + FP)$$

where *True Positive (TP)* means the pixel is correctly identified as part of a building/crater object; *False Positive (FP)* means that a pixel is incorrectly identified as part of a building/crater object but is actually background; *False Negative (FN)* means that a pixel is incorrectly identified as part of the background when it is actually part of a building/crater object.

However, there are problems with using these metrics for automated crater detection because of the lack of reliable ground truth at the relevant resolution.

Therefore two processing stages are undertaken:
Stage 1. Edit and Assessment
- read each detection result from a text file & create a polygon shapefile containing each crater result
- overlay each shapefile on its base image for manual verification & digitisation
- tag TP, FP and delete FNs
- establish the crater diameter lower limit cut-off in pixels for assessing the algorithm performance
- compile the data and calculate statistics quantifying the performance for each image and detection result

Stage 2. Merge and create 2D GIS file
- merge the crater data sets from Stage 1.
- resolve duplicates where orbital images overlap
- produce a merged, georeferenced 2D crater shapefile

In order to establish a detection cut-off minimum diameter in pixels, the detection metrics are calculated as a function of diameter. Plots of detection percentage against diameter in pixels are constructed and the cut-off minimum crater diameter in pixels for the chosen level of detection is determined. The assessment metrics are then calculated by only counting craters with diameters greater than this cut-off value. A cut-off limit of 8 pixels was selected as representing the algorithm's current limits for acceptable detection and quality rates, representing diameters of 320 metres and 200 metres for Elysium and Iani respectively as shown in Figure 6. Assessment results obtained for the Elysium and Iani images are shown in Table 2.
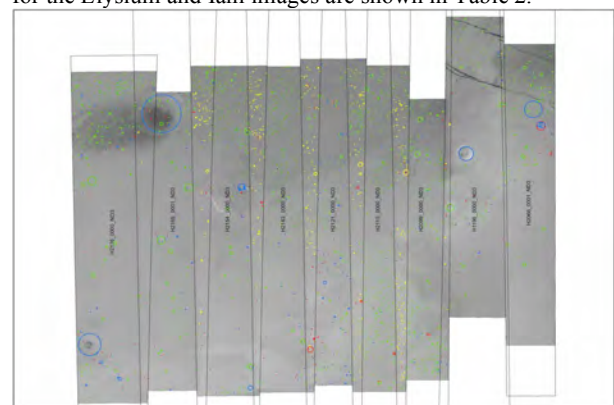
(a) 2,543 Craters for the image strips in Elysium Planitia
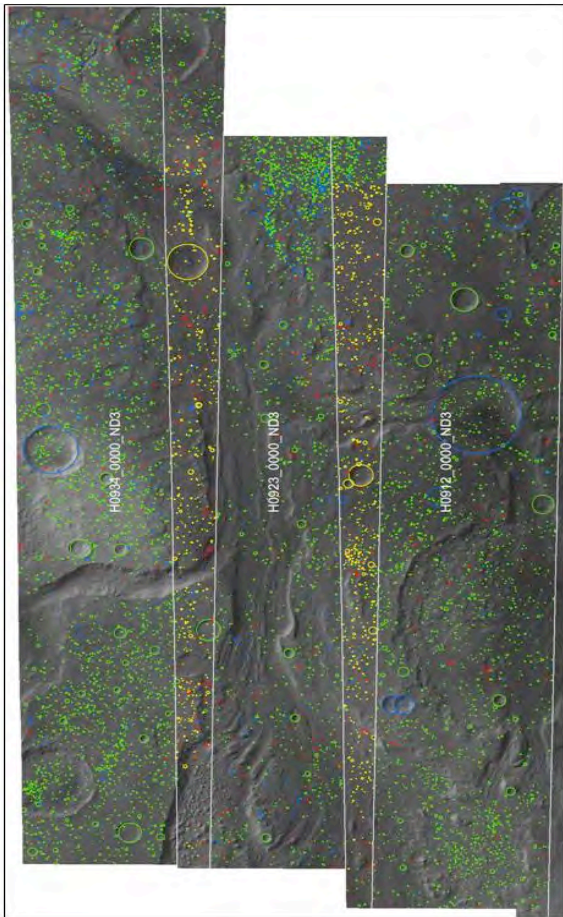
(b) 8,857 Craters for the image strips in Iani Vallis
Figure 6. Crater Detection results and assessment.
Green = True Positives, Red = False Positives (not in count),
Blue = False Negatives, Yellow = Interpolated from duplicates

Region	Mean % Detection	Mean % Quality	Mean Branching Factor
Elysium	85.59	80.09	0.09
Iani	83.31	77.74	0.09
Overall	84.45	78.92	0.09

Table 1. 2D crater assessment results (diameter ≥8 pixels).

3.2 Assessment of 3D crater profiles

The assessment of 3D craters was performed in three ways: 1) an inter-comparison between optical images and hill-shaded images based on reconstructed DTMs, or constructed DTMs and standard 3D models; 2) manual check; 3) comparison with other 3D information sources such as HiRISE, CTX and MOLA track profiles.

At first the inter-comparison between optical images and DTM was designed for a kind of automated verification stage of the 3D processing. The hill shaded image was constructed using the illumination conditions from the corresponding HRSC image and a correlation value with median filtered optical images was derived. A thresholding value to discriminate ill-constructed DTM is roughly > 0.35 but depends on crater size. We used 0.35-0.5 depending on crater size. In addition, the convolved value between the constructed DTM with pre-defined standard 3D models was checked. If the maximum convolved value with a standard DTM is lower than 0.7, it is classified as a poor case.

We processed 40 craters (r>400m) over parts of HRSC images h1190, h2099 and h1923. Figure 7 and Table 2 show some examples of 3D crater DTM and the assessment results.
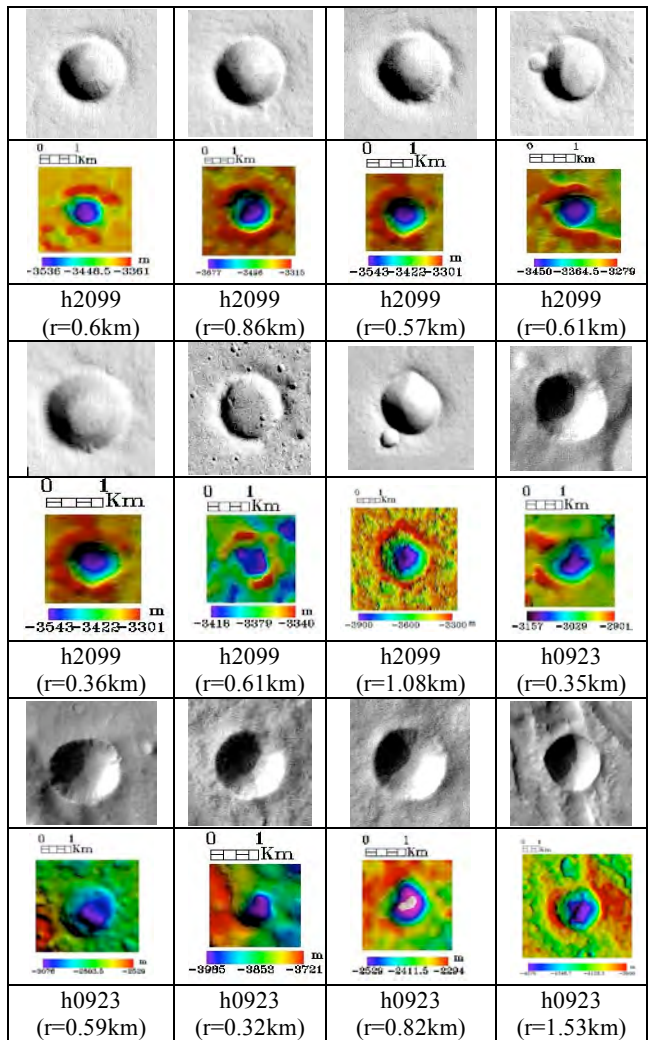

Figure 7. Hill shaded images of individual crater DTMs

	Automated Verification[a]	Manual verification[b]	Manual verification[c]
Overall detection	76.6%	96.6% DP :78.5% BF : 0% QP :78.5%	86.6% DP :88% BF : 0% QP :88%
r>1000m	100%	100%	100%
1000m<r<450m	73.3%	100%	86.7%
r<450m	70%	80%	90%

(a) HRSC orbit 2099 (29 crater DTMs)

	Automated Verification[a]	Manual verification[b]	Manual verification[c]
Overall detection	40.9%	81.8% DP :41.1% BF : 0.14 QP :38.8%	54.5% DP : 45.4% BF : 0.6 QP : 35.7
r>1000m	66.6%	66.6%	50%
1000m<r<450m	27.2%	90.9%	63.6%
r<450m	40%	80%	40%

(b) HRSC orbit 0923 (21 crater DTMs)

[a] using DTM and hill shading
[b] manual check, if depth/diameter is available, true
[c] manual check if crater rim is clear, true

Table 2. Assessment results of crater DTMs (crater diameter≥8 pixels). DP : detection percentage compared with automated verification and manual verification standards, BF : branching factor, QP ; quality percentage. See equations in section 3.1

According to these assessment result, the resolution limit of 3D crater extraction algorithms is *radius* >500m and *depth* <70m with HRSC stereo images.
Finally to check the quality of the constructed crater DTM, a few of them were compared with CTX (10m) stereo DTMs. The method to build CTX is described in Kim and Muller (2007). Even though the availability of such DTMs is very limited at present, it provides a good insight into the reliability of the crater matching system as shown in Figure 8 .


| CTX 10m DTM | HRSC 20m DTM orbit 2099 (r=0.98km) | Blue : CTX, Red: HRSC DTM profile |
| CTX 10m DTM | HRSC 20m DTM orbit 2099 (r=0.41km) | Blue : CTX, Red: HRSC DTM profile |
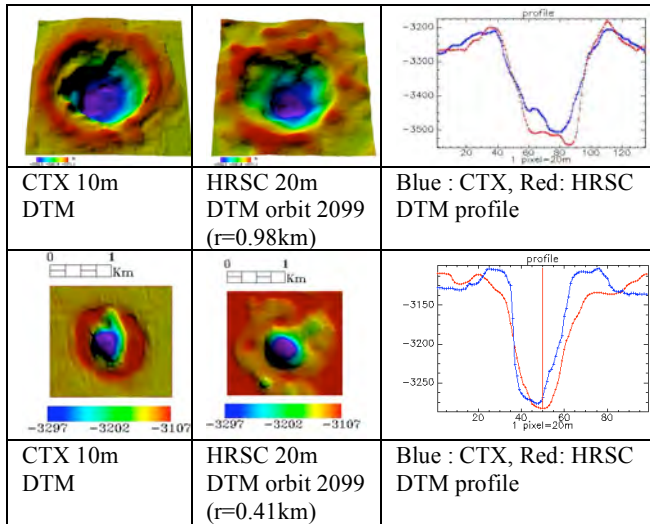
Figure 8. The DTM comparison with CTX (note stereo height difference inferred to come from the influence of illumination angle)

4. CONCLUSIONS & FUTURE WORK

We showed an implementation of an automated and semi-automated crater GIS construction. There have been several previous studies on automatic impact crater detection algorithms but we believe this is the first case to incorporate crater detection algorithms into a practical crater GIS data generation systems. As shown in the 2D GIS assessment, a completely reliable and automated crater detection method is not available yet. This is believed to be mainly due to the accuracy of the verification method being insufficient. We described the software tools for editing and merging to compensate for any weakness in the construction of crater GIS. Moreover, we demonstrated a comprehensive system developed for the automated 3D crater DTM. The assessment shows that the data fusion method produced reliable 3D information on individual craters. The 2D crater GIS was produced over very extensive areas including the whole of Iani and Elysium. It is expected that the processing software will provide a very powerful tool for research in surface dating and geomorphological analysis. On the other hand, the general approach to update the performance of this system will be continuously explored through enhanced 3D construction algorithms such as shape from shading. In addition, the employment of HiRISE and CTX stereo data sets for creating finer resolution 3D crater GIS data is now being explored to allow finer-scale detail to be obtained for testing different models of crater size frequency distributions and surface age to be tested.

REFERENCES

Barlow, N. G. et al, 2003. Utilizing GIS in Martian impact crater studies. I*nternational Society for Photogrammetry and Remote Sensing Working Group IV/9: Extraterrestrial Mapping Workshop, "Advances in Planetary Mapping 2003", 22, March, 2003, Houston, Tx, USA,* http://astrogeology.usgs.gov/Projects/ISPRS/MEETINGS/Houston2003/abstracts/Barlow_isprs_mar03.pdf

Cheng, Y. et al, 2003. Optical landmark detection for spacecraft navigation. *Proceedings of the 13th AAS/AIAA Space Flight Mechanics Meeting. Ponce, Puerto Rico, AAS.*

Fitzgibbon, A. W., Pilu, M., and Fisher, R. B. 1996. Direct Least Squares Fitting of Ellipses. *IEEE Transactions on Pattern Analysis and Machine Intelligence.* 21(5), pp. 476-480.

Gruen, A. 1985. Adaptive Least Squares Correlation: A powerful Image Matching Technique. *South Africa Journal of Photogrammetry, Remote Sensing and Cartography.*14(3), pp. 175-187.

Hartmann, W. K., 1966. Martian cratering. *Icarus 5*, pp. 565-576.

Kanatani, K., Ohta, N., 2004. Automatic detection of circular objects by ellipse growing, *Int. J. Image Graphics*, 4(1), pp. 35–50.

Kim, J. R., 2005. Landscape Object Detection and Reconstruction by Multi-sensor Data Fusion. *PhD. Department of Geomatic Engineering, University College London (unpublished).*

Kim, J. R. et al, 2005. Automated Crater Detection, A New Tool for Mars Cartography and Chronology. *Photogrammetric Engineering & Remote Sensing*, 71 (10*)*, pp. 1205-1217.

Kim, J. R. and Muller, J.-P., 2007. Very high resolution DTM Extraction from HiRISE Stereo Imagery, *European Mars Science and Exploration Conference, 12-16, Nov, 2007, Noordwijk, Netherlands,* http://sci.esa.int/science-e/www/object/index.cfm?fobjectid=41364&fbodylongid=1991

Salamuniccar, G. and Loncaric, S., 2007. Open framework for objective evaluation of crater detection algorithms with first test-field subsystem based on MOLA data. *Advances in Space Research, In Press, Corrected Proof.*

Scholten, F.,et al 2005. Mars Express HRSC Data Processing–Methods and Operational Aspects, *Photogrammetric Engineering & Remote Sensing*, 71 (10), pp. 1143-1153.
Shufelt, J. A., 1999. Performance evaluation and analysis of monocular building extraction from aerial imagery. *Ieee Transactions on Pattern Analysis and Machine Intelligence*, 21, pp. 311-326.

Turk, M., and Pentland, A. 1991. Eigenfaces for Recognition. *Journal of Cognitive Neuroscience,* 3, pp. 71-76.

Vinogradova, T. et al, 2002. Training of a crater detection algorithm for Mars crater imagery. *Aerospace Conference Proceedings, 2002. IEEE*, 7, pp. 3201-3211 .